Adaptive Optics: Observations and Prospects for Studies of Active Galactic Nuclei

Richard Davies

Max-Planck-Institut für extraterrestrische Physik, Garching, Germany

Abstract

These lectures take a look at how observations with adaptive optics (AO) are beginning to influence our understanding of active galactic nuclei (AGN). By focussing on a few specific topics, the aim is to highlight the different ways in which enhanced spatial resolution from AO can aid the scientific analysis of AGN data. After presenting some background about how AO works, I will describe a few recent observations made with AO of QSO host galaxies, the Galactic Center, and nearby AGN, and show how they have contributed to our knowledge of these enigmatic objects.

Key words: instrumentation: adaptive optics, Galaxy: center, galaxies: active, galaxies: kinematics and dynamics, galaxies: nuclei, galaxies: Seyfert, galaxies: starburst, quasars: general, infrared: galaxies
PACS: 95.85.Jq, 98.35.Jk, 98.54.Aj, 98.54.Ep, 98.54.Cm, 98.62.Dm, 98.62.Js

1 Introduction

Adaptive Optics (AO) serves two purposes. It is an enabling technology for even more complex instrumentation such as IR/optical interferometry. But it is also an important technique in its own right. At near-infrared wavelengths (1–5 μm) it allows one to improve the spatial resolution of ground-based telescopes by an order of magnitude from 0.5–1″ to the diffraction limit, which for an 8-m class telescope in the H-band (1.6 μm) is about 40 mas. AO has applications in many areas of astronomy because it not only increases a telescope's sensitivity for unresolved sources, but it also reduces crowding problems in dense fields, and sharpens our view of the morphologies and kinematics of extended objects. In these lectures, the impact that adaptive optics is having on studies of Active Galactic Nuclei (AGN) is discussed with particular reference to three topics

Email address: davies@mpe.mpg.de (Richard Davies).

that span scales from $< 1\,\mathrm{pc}$ in the innermost region of our Galactic Center, through 10 pc scales in nearby AGN, to kpc scales in QSO host galaxies at high redshift. By studying these different aspects and combining what we can learn from different spatial scales, we can gain a more holistic view of the structures comprising AGN and the physical processes governing how they are fuelled.

2 Adaptive Optics Overview

It is only by understanding the basic ideas behind adaptive optics that one can make the best use of it. This section therefore begins by looking at the effect that atmospheric turbulence has on a propagating wavefront. By making the approximation that the turbulence occurs in a thin layer at a fixed height, it addresses how adaptive optics can correct these aberrations. And it provides the tools needed to make simple quantitative statements about the impact of adaptive optics on a series of observations. Some ways in which the major limitations are being overcome are briefly considered.

2.1 Atmospheric Turbulence

The atmosphere is a dynamically active structure which constantly has energy injected into it, either through heating (e.g. direct sunlight or re-radiation from the ground) or via convection currents and wind shear. These effects occur on scales of several tens of metres (the outer scale, L_0), and the energy is gradually transferred to smaller scales, until it is dissipated on scales of a few millimetres (the inner scale, l_0). This leads to local variations in the temperature and density of the air, and hence in its refractive index n. It can be quantified statistically using the structure function which describes the difference in n between a location r' and another location separated from it by r. For Kolmogorov statistics, the refractive index structure function is defined in terms of an average – denoted $\langle\rangle$ – over all possible r' and r. It takes the form

$$D_n(r) \;=\; \left\langle [n(r') - n(r'+r)]^2 \right\rangle \;=\; C_n^2 r^{2/3} \tag{1}$$

where C_n^2 is the refractive index structure constant. It is notable that the $r^{2/3}$ here is the origin of all the $\frac{1}{3}$ powers in expressions associated with adaptive optics. As it stands, this expression implies that the refractive indices at two points decorrelate ever more as the separation between the points increases. But this is true only as long as $r < L_0$ (e.g. for 2-m or 4-m telescopes). Instead,

the decorrelation reaches a maximum at $r = L_0$, and the effect of this can be measured even on an 8-m telescope. As a result, the van Karman model is more often used. This is the same as the Kolmogorov model, but takes into account the inner and outer scales.

The impact that $D_n(r)$ has on a wavefront propagating down through the atmosphere is described using the phase structure function

$$D_\phi(r) \;=\; 2.91 \left(\frac{2\pi}{\lambda}\right)^2 (\sec\zeta)^{5/3} \int_0^\infty C_n^2(h) dh \tag{2}$$

a good derivation of which is given by Roddier (1981). In this equation, ζ is the angular zenith distance at which one is looking, since the $C_n^2(h)$ profile is defined vertically through the atmosphere. In the most simple approximation, one can think of the atmosphere as a single thin 'phase screen', which induces a relative (phase) delay between two different points on a wavefront that depends only on the lateral separation of those points.

An important quantity to introduce here is Fried's parameter r_0 (Fried, 1965), which describes the coherence length of the atmosphere and is defined as

$$r_0 \;=\; 0.185\ \lambda^{6/5} (\sec\zeta)^{3/5} \left(\int_0^\infty C_n^2(h) dh\right)^{-3/5} \tag{3}$$

Put in simple terms, r_0 is the size of aperture (e.g. telescope mirror) across which a wavefront can, for practical purposes, be considered unperturbed. In fact, the variance σ^2 of the resulting wavefront aberrations over a circular aperture of diameter D can be expressed in terms of Fried's parameter as

$$\sigma^2 \;=\; 1.030 \left(\frac{D}{r_0}\right)^{5/3} \tag{4}$$

Thus 'unperturbed' means having only $1\,\mathrm{rad}^2$ of variance. The immediate conclusion one can draw from this equation is that turbulence limits the resolution of a telescope to λ/r_0 instead of λ/D. Other important parameters can be derived from r_0, two of which are the coherence timescale τ_0 and the isoplanatic angle θ_0. However, note that in reality these parameters are much less well correlated than implied here.

The coherence timescale can be thought of as the temporal equivalent of r_0, and is related to the time taken for the wind to blow across a cell of size r_0. Specifically, it is the time over which the variance of a wavefront changes by $1\,\mathrm{rad}^2$. It is defined assuming Taylor's frozen flow hypothesis which asserts

that temporal changes in the turbulence along a line of sight are due only to the lateral shift of an otherwise fixed phase screen. It is given as

$$\tau_0 \;=\; 0.314 r_0 / V_{wind} \;\text{ where }\; V_{wind} \;=\; \left[\int_0^\infty C_n^2(h) v^{5/3} dh \Big/ \int_0^\infty C_n^2(h) dh \right] \quad (5)$$

where v is the wind velocity as a function of height, and hence V_{wind} is a weighted mean wind velocity.

The isoplanatic angle is related to the angular size of r_0, which depends on the weighted mean distance H to the phase screen that we are using to approximate the atmosphere. Specifically, it is the angular distance between two lines of sight which causes the wavefront variance to change by $1\,\mathrm{rad}^2$, and is defined as

$$\theta_0 \;=\; 0.341 r_0 / H \;\text{ where }\; H \;=\; \sec\zeta \left[\int_0^\infty C_n^2(h) h^{5/3} dh \Big/ \int_0^\infty C_n^2(h) dh \right]^{3/5} \quad (6)$$

As we shall see later, the three parameters above form the basis for estimating the wavefront variance due to the atmosphere: r_0 and τ_0 describe the ambient atmospheric conditions and hence how well the AO system is likely to perform, while θ_0 describes how much the performance will degrade as one moves off-axis from the guide star. They all depend on $C_n^2(h)$, so that some knowledge of the turbulence profile (refractive index structure constant) through the atmosphere is needed. Various models for how $C_n^2(h)$ varies with height are available, each typically including a strong ground layer and then more moderate turbulence distributed in layers up to a height of 10–20 km. Direct measurements of $C_n^2(h)$ now typically form a crucial part of the site characterisation for any modern telescope.

2.2 Impact of a Perturbed Wavefront

After passing through the atmosphere, a wavefront that was originally planar will be corrugated. As such, the normal vectors at different points – i.e. the direction in which the photons are propagating – are no longer parallel. The direct result is that they can no longer be brought to focus at a point, and instead form a blur. This is quantified by the point spread function (PSF), which is the image produced by an optical system of an unresolved source . If a plane wavefront propagates through a circular entrance aperture (pupil) and is focussed by perfect optics, the image will be an Airy function which shows clear diffraction rings. Mathematically, the pupil and PSF are related via the optical transfer function (OTF) which describes how well different

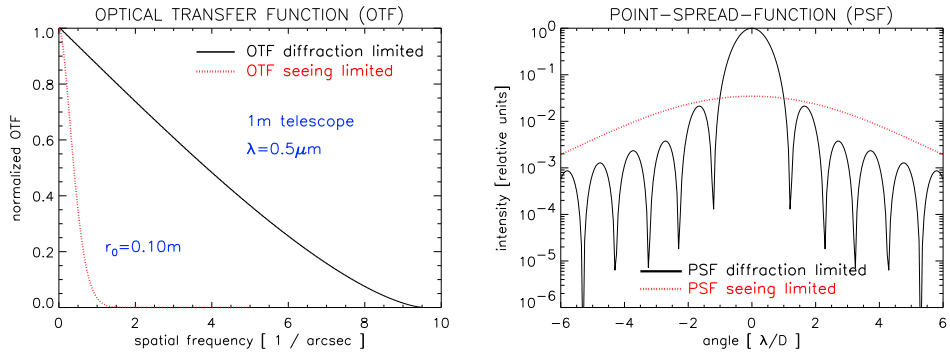

Fig. 1. Optical Transfer Function (left) and Point Spread Function (right) for perfect optics giving diffraction limited imaging, and also for a perturbed wavefront. The OTF and PSF are Fourier Transforms of each other; for a plane wavefront propagating through perfect optics, the OTF is the auto-correlation of the (entrance) pupil. From Egner (2006), courtesy of S. Egner.

spatial frequencies are transferred through the optical system. The OTF is the autocorrelation of the pupil, and the PSF is the Fourier transform of the OTF. As Fig. 1 shows, for a circular pupil, the OTF is very nearly a conical function. A strongly perturbed wavefront will yield only a more diffuse PSF, which is often characterised by a Gaussian function (albeit with broader wings). In this case, the OTF is also approximately Gaussian, and shows that high spatial frequencies are not transmitted through the imaging system (i.e. the atmosphere).

2.3 A Simple Adaptive Optics System

To flatten a wavefront that has been corrupted by the atmosphere, an AO system must include a wavefront sensor (WFS) to measure the shape of the wavefront and a deformable mirror (DM) with which to apply the corrections (although for practical purposes the global slope, or tip-tilt, is usually corrected by a separate flat mirror). What happens can be seen in Fig. 2. The perturbed wavefront is reflected from the initially flat DM into the WFS. Here, the shape of the wavefront is measured, and a real-time computer turns these measurements into a set of commands (i.e. voltages) which are sent to the DM. The DM can now correct the shape of the wavefront to be what it was a short time previously (at least to the limits of the WFS sensitivity and mechanical ability of the DM). Thus, what remains is only a small residual wavefront aberration due to changes since the previous measurement was made. It is this residual aberration that is now measured by the WFS, and a correction is made to update the DM commands. This update cycle of only the residual wavefront error is known as ‘closed loop’ operation.

The fact that the wavefront is sensed at optical wavelengths, while the science

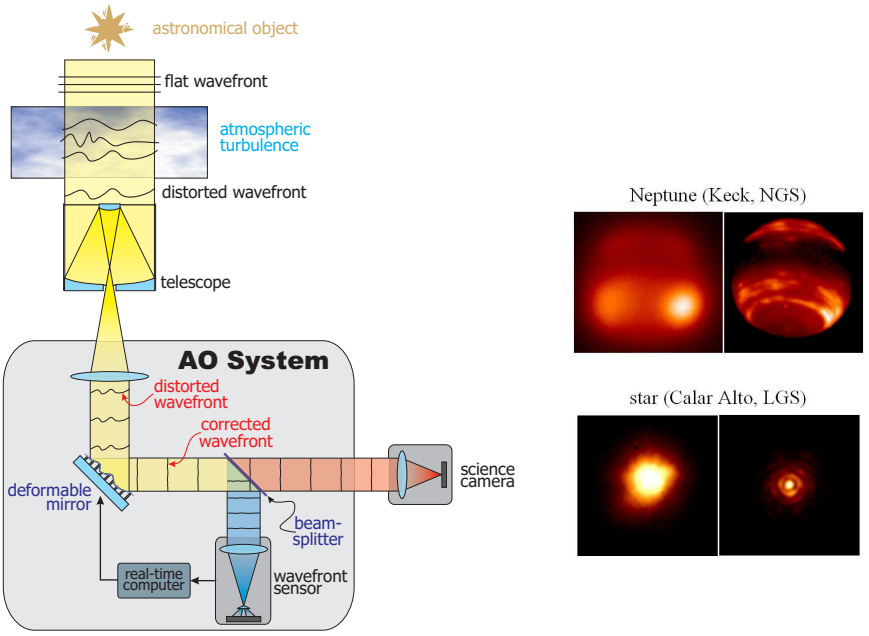

Fig. 2. Left: a cartoon showing the principle of a simple AO system; from Egner (2006), courtesy of S. Egner. Right: examples of seeing limited and corrected images. Top: Neptune, taken on the Keck telescope using NGS, courtesy of C. Max; Bottom: a star corrected with the LGS-AO system ALFA, showing diffraction rings, adapted from Davies et al. (2000).

channel is infrared implicitly assumes that the same correction is valid for both wavelengths. This is true because the wavefront aberrations are simply shifts in longitudinal position of the wavefront at different places. And a shift (i.e. delay) of, say, 100 nm is the same whether it applies to infrared or optical photons. The wavelength dependence arises from the impact of this delay: 100 nm is $\lambda/5$ in the optical, but it is only $\lambda/20$ in the near infrared and hence has less effect there. We have already seen this in Fried's parameter, Eq. 3 showing that $r_0 \propto \lambda^{6/5}$. Thus, at longer wavelengths, the coherence length and timescales are longer. As such, the image quality is not degraded so much, and adaptive optics can work better.

Perhaps one surprising feature of AO is the speed (frame rate) at which the wavefront must be measured in order to correct it, as demonstrated in Fig. 3. Typically, the bandwidth (i.e. the frequency below which aberrations are well corrected) is about 1/10 the frame rate. This becomes apparent when comparing τ_0 to the Greenwood frequency f_G, which is defined from the engineering perspective as the closed loop bandwidth at which the residual wavefront variance is $1\,\mathrm{rad}^2$. One finds that $1/\tau_0 = 7.5 f_G$, a difference that is due to the inevitable time delay that arises because a correction can only be applied after it has been measured. If the AO system has a frame rate of 100 Hz, the shape of the DM can only be updated at least 10 ms after the measurement of the wavefront residual has started. It means that algorithms which can predict

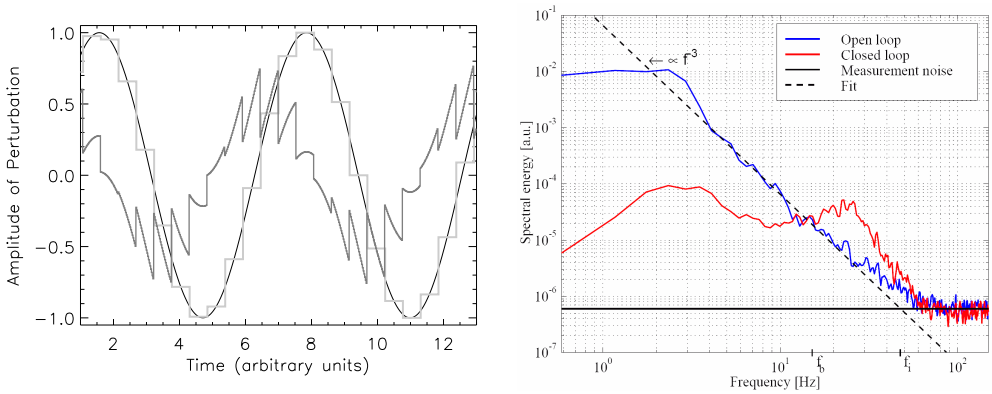

Fig. 3. Left: Illustration showing that if a perturbation (black line) is sampled at 12 times the speed at which it changes (light-grey line), the strength of the residual (dark grey line) is reduced by only a factor 2 but also exhibits higher frequency perturbations. Right: Data measured with the ALFA AO system showing that in close loop, the low frequency perturbations are corrected, but extra energy is put into the higher frequencies. The AO system was running with a frame rate of 300 Hz but the closed loop bandwidth f_b is only 15 Hz. The noise floor f_i is reached at about 50 Hz. From Kasper (2000), courtesy of M. Kasper.

what shape the wavefront will have even a short time in the future, could yield a significant improvement in AO performance. This issue, however, is rather complex because the atmosphere consists of multiple layers moving in different directions, and there is no easy way to make a sensible prediction unless the different layers can be sensed separately. It is therefore reassuring that some progress is being made in this direction using Fourier techniques (Poynier et al., 2007).

2.4 Wavefront Sensors

There are a number of ways of measuring the shape of the wavefront, the two most commonly employed of which are the Shack-Hartmann sensor (developed by Shack & Platt 1971, based on a device originally devised by Hartmann 1900) and the curvature sensor (Roddier, 1988).

A Shack Hartmann sensor uses an array of lenslets to split the pupil into a series of sub-apertures, and is easy to extend to very high order. However, the geometry cannot be adjusted to match the ambient seeing conditions, and the resolution is limited by the sub-aperture size rather than the full pupil. It works by creating an image of a star through each sub-aperture, the position of which depends on the local wavefront slope. The combination of all of these local slopes yields the global first derivative of the wavefront. Such systems are typically used with a DM consisting of a series of individual piezo actuators, across which is glued a thin flexible mirror. The actuator lengths change as

voltages are applied, generating local gradients across the mirror surface.

A curvature sensor measures the second derivative of the wavefront. It does this by comparing slightly pre- and post-focal images of the star, and the difference in intensity at each point yields the local wavefront curvature. This type of sensor is usually used with a bi-morph mirror, consisting of a 2-layer piezo ceramic, one surface of which is silvered. It bends when a voltage is applied at a certain point, naturally reproducing the measured curvature. Although it is harder to make high order systems this way, there are a number of advantages: the sensitivity can be adjusted at any time by modifying how afocal the two reference images are; and the aperture is not divided, so one can benefit from the higher resolution achieved in closed loop.

2.5 Residual Wavefront Variance

In Section 2.1 we saw how r_0, τ_0, and θ_0 could be estimated from a measurement of $C_n^2(h)$ in the atmosphere. These characterise the spatial and temporal distortions of the incoming wavefronts, which are then measured and corrected by an AO system which itself has some spatial and temporal limitations. Using these, one can estimate how the corrected PSF should look – and quantify it in terms of the Strehl, the ratio of the actual peak intensity to that which would be achieved with a perfect optical system.

Spatial wavefront distortions are usually characterised in terms of orthonormal basis functions, the simplest of which for a circular aperture are the Zernike modes. The first few low order Zernike terms describe the well known effects of piston, tip-tilt, astigmatism, focus, coma, and trefoil. However, since telescope apertures are annular, and annular Zernike modes are not orthonormal, in practice the more complex Karhunen-Loève modes are used. Only a finite number of modes can be corrected (no more than about 2/3 the number of measurements made), leaving a residual wavefront variance

$$\sigma_{fit}^2 \;\sim\; 0.2944 j^{-\sqrt{3}/2} (D/r_0)^{5/3} \tag{7}$$

where j is the number of (Zernike) modes corrected. The expression is valid for large j; variances for small j are given in Beckers (1993). The residual variance due to the limited bandwidth of the AO system can be estimated as

$$\sigma_{lag}^2 \;=\; (\tau/\tau_0)^{5/3} \tag{8}$$

where τ is the time lag from the start of a measurement with the WFS to the time at which it is applied to the DM. And finally, the residual variance which

occurs if the science target is a finite angular distance θ from the guide star is

$$\sigma^2_{angle} \;=\; (\theta/\theta_0)^{5/3} \tag{9}$$

There are inevitably other constraints on the performance of any AO system, such as the photon and read noise in the measurement. These depend on the design and hardware of each specific system and are discussed more elsewhere (e.g. Hardy, 1998). Although beyond the scope of this brief overview, they need to be included in the estimate of the total variance which is then used to estimate the Strehl S with the approximation

$$S \;\sim\; e^{-\sigma^2_{total}} \;\text{ where }\; \sigma^2_{total} \;=\; \sigma^2_{fit} + \sigma^2_{lag} + \sigma^2_{angle} + \sigma^2_{noise} + ... \tag{10}$$

Some typical values for the K-band ($2.2\,\mu$m) Strehl on an 8-m telescope are: 1–2% for the seeing limit; 20% for reasonable performance; 50% with on-axis bright stars; and $> 90\%$ is the aim for the generation of extreme AO systems currently being designed.

2.6 Sodium and Rayleigh Laser Guide Stars

The major limitation with natural guide star (NGS) AO is that for good performance one needs a star brighter than $V \sim 13\,$mag – and the probability of finding one close to any particular science target is very low. As a result, the isoplanatic residual variance σ^2_{angle} often dominates the error budget. To keep this term under control, the sky coverage for NGS-AO is limited to at most a few percent, and far less at the galactic pole. The alternative is to generate an artifical star, which one can point anywhere in the sky. This can be done by projecting a high quality and high power laser beam into the sky and measuring the back scattered light. Rayleigh lasers (usually green or UV) are pulsed and one can gate the detector so it sees each pulse of light scattered by the air at a specific altitude, usually in the range 10–30 km. Sodium line lasers (orange) are designed to make the layer of neutral sodium atoms at a height of $\sim$90 km fluoresce. Although using a laser to create an artifical star does to a large extent solve the isoplanatic issue, it also brings its own problems.

A Rayleigh laser system is relatively straightforward to construct. However, for 8-m class telescopes there is a major limitation known as the cone effect (or focal anisoplanatism). Because the LGS is at a finite height, its light only samples a conical volume along the line of sight, whereas light from a distant astronomical object traverses a cylindrical region through the atmosphere. This means that much of the turbulence is not sensed and so cannot be corrected. To avoid this issue, one can either use multiple guide stars (see Section 2.7) or create a guide star much higher up in the atmosphere.

For this reason, sodium line lasers are a popular option. However, a major issue is the technology needed to build them. As yet there is no robust turn-key laser that can produce of order 10 W at 589 nm. In addition, the mesospheric sodium layer is rather thick (typically 10 km) and so any spot seen off-axis will be elongated – a critical issue even on 8-m class telescopes if the laser is not projected from behind the secondary mirror. Furthermore, the sodium layer is a dynamic entity, and the number of atoms is very variable, impacting the brightness of the spot. But also the mean height can vary rapidly, dominating over the change in height due to tracking across the sky. If one does not correct for both of these, one can accumulate significant focus residuals. Finally, as for Rayleigh lasers, one still needs a NGS to correct for tip-tilt since this cannot be measured with an LGS (the laser accumulates an unknown tip-tilt as it propagates upward through the atmosphere). While a tip-tilt NGS can be fainter and further from the science object than one used for high order AO correction, it is still a significant constraint. As yet, none of the solutions proposed have been satisfactory. As an alternative, it has been suggested to dispense with tip-tilt if one does not need to reach the diffraction limit (Davies et al., 2008).

2.7 Multi-Conjugate Adaptive Optics

The residual variance due to isoplanatism not only limits the sky coverage – which led to the development of LGS – but it limits the field of view that can be corrected. At Paranal, the typical K-band isoplanatic angle is only 12.7″ (Cresci et al., 2006), so even at this distance from the guide star the Strehl is much reduced. This obstacle can be surmounted using multi-conjugate adaptive optics (MCAO). Here one uses multiple laser (or natural) guide stars to fully sample the turbulence. With a tomographic reconstruction, one can then approximate the atmosphere as several phase screens at different heights. It is then possible to use two or more DMs, each conjugated to a different layer, to perform a full correction on the wavefront that works even off-axis. Essentially what is happening is that off-axis rays reflect off the DMs in different places to an on-axis ray, and hence receive different total corrections that are appropriate for their path through atmosphere. Over recent years, there has been a considerable effort in this direction, leading to two concepts for MCAO systems. The first uses classical tomography: the wavefront errors for each guide star are sensed separately; and the measurements are combined in a computer which calculates how much phase delay occured at each point in each layer. In layer oriented MCAO (Ragazzoni et al., 2000), the light from the guide stars is combined optically on the detectors, and there is one detector associated with one DM for each layer that is corrected. For this design, each layer/detector/DM combination is an independent AO loop, and hence the whole system is computationally much simpler.

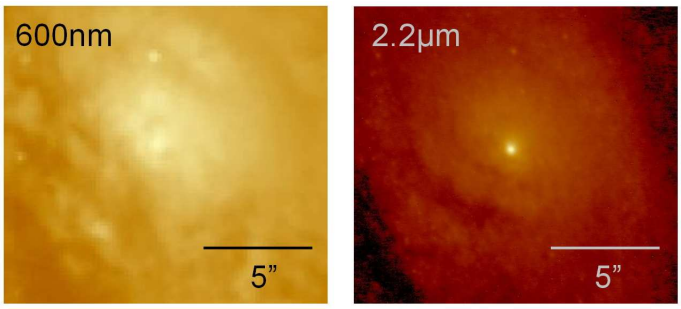

Fig. 4. Optical and near infrared views of the nucleus of the Circinus galaxy, on a logarithmic scaling. While the nucleus is faint and fuzzy at 600 nm, there is a bright compact source suitable for an infrared WFS at 2.2 μm. Optical image courtesy of the *HST* archive; infrared image from Prieto et al. (2004).

Although a proto-type MCAO system for solar astronomy was tested in the last few years on a small telescope, the first one for an 8-m class telescope became operational only recently (MAD, Marchetti et al., 2007). During the next few years, several others should become operational on Gemini South, the Very Large Telescope, and the Large Binocular Telescope.

2.8 Realistic Expectations

The discussion so far has assumed that the AO guide star is just that: a star. So what should we expect for AGN, which in general are not particularly bright, are often fuzzy at optical wavelengths, and have a relatively bright background due to the host galaxy? One of the clearest examples of this problem is the Circinus Galaxy. Fig. 4 shows that at optical wavelengths there is almost nothing to use as a wavefront reference, and so AO cannot perform well. It is hard to predict what performance one should expect using an AGN itself as the wavefront reference. In such cases, one can often do much better than the seeing limit, but one should certainly not expect perfect performance every time. Fortunately, Circinus does have a bright compact near infrared source suitable for AO guiding if one has an infrared wavefront sensor like that in NACO on the VLT. Alternatively – and more commonly – one will have to use a laser guide star. But one should be aware that with current LGS facilities, one can get anything from 0.1″ resolution to ∼30% Strehl in the K-band depending on the ambient conditions. It is worth remembering that LGS-AO is still in its infancy, and there are likely to be many improvements in future generations of LGS-AO systems that should lead to greater efficiency and better performance for more of the time.

3 Quasar Host Galaxies

Armed with some knowledge about adaptive optics, we can explore where it can make the biggest impact in studies of AGN. We begin with QSOs, where the aim has been to detect and measure the properties of their host galaxies. We highlight cases where AO has started making an impact on this topic, and discuss the implications of this work in the context of where the most powerful QSOs reside, and of the possible evolutionary scenario linking them to ultraluminous galaxies (ULIRGs).

3.1 What can we learn from QSO Host Galaxies?

Since its discovery, the relation between the mass $M_{\rm BH}$ of the black hole in the center of a stellar spheroid and the velocity dispersion σ_* of that spheroid (Ferrarese & Merritt, 2000; Gebhardt et al., 2000) – which superseded similar ones using the luminosity or mass of the spheroid (Kormendy & Richstone, 1995; Magorrian et al., 1998) – has become a cornerstone for cosmological models. It is generally accepted that the $M_{\rm BH} - \sigma_*$ relation should be valid for all spheroids irrespective of mass-scale, environment, and evolutionary history – for example, whether the black hole is quiescent or active, whether the spheroid is embedded in a gaseous disk or not, or whether it is a giant elliptical or a globular cluster. This interpretation is bolstered by evidence that moderate mass systems such as Omega Centauri host intermediate mass black holes (Noyola et al., 2008). And it only makes sense if black holes grow at the same rate as the bulges in which they reside. It is this pretext that currently forms the basis for our understanding of galaxy evolution and black hole growth.

Over the last decade there has also been an intense effort to derive the evolution with cosmic time of both the star formation rate density and the number density of luminous QSOs. Remarkably, these both follow qualitatively similar trends and both peak around $z \sim 2$–3, at least indicative that stars and AGN do indeed evolve and grow in parallel. However, as always there are a few glaring exceptions, of which perhaps the most spectacular is the $z = 6.4$ QSO J1148+5251. Continuum and emission line scaling relations yield $M_{BH} = (1 - 5) \times 10^9\,{\rm M}_\odot$ (Fan et al., 2003). But the fact that such a massive black hole can exist so early in the universe implies sustained and very rapid growth. To add to the puzzle, interferometric observations of the molecular gas in this object were able to resolve the CO(3-2) line spectrally and spatially (Walter et al., 2004) . They revealed two peaks separated by 1.7 kpc. Assuming that these are gravitationally bound with a rotational velocity corresponding to the $280\,{\rm km\,s^{-1}}$ FWHM of the line, the dynamical mass of the system is $\sim 5 \times 10^{10}\,{\rm M}_\odot$. This is more than an order of magnitude less

than the $\sim 10^{12}\,\mathrm{M}_\odot$ implied by the $M_{\rm BH} - \sigma_*$ relation. This result suggests that at early times, black holes may form before stellar bulges are assembled.

It is to understand more about the $M_{\rm BH} - \sigma_*$ relation and its relevance and implications for cosmic evolution that we need to study QSOs and their host galaxies. One way to do this is to look at local relic populations and infer what must have happened to create them; or we can look directly at high redshift QSOs where the action is actually taking place.

3.2 How can we study QSOs and their Hosts?

At low redshift one can use reverberation mapping (RM) to derive $M_{\rm BH}$ by equating it with the virial product of the width of an emission line from the broad line region (BLR) and the time delay with which its flux follows changes in the UV continuum (Peterson, 2001). Secondary relations then make use of the apparent scaling between the size of the BLR and the optical continuum luminosity (Kaspi et al., 2005) to extend the RM technique to higher redshift, using the virial product of an emission line FWHM and the BLR size. This is simply asserting that $M \propto \sigma^2 R$ which, when calibrated, becomes (Vestergaard, 2004)

$$\log \frac{M_{BH}}{M_\odot} \;=\; 6.7 + 0.7 \log \left(\left[\frac{\mathrm{FWHM(H}\beta)}{1000\, km\, s^{-1}} \right]^2 \left[\frac{\lambda L_\lambda (5100\text{Å})}{10^{44}\, erg\, s^{-1}} \right]^{0.7} \right) \qquad (11)$$

The Eddington rate L_{bol}/L_{Edd} can then be found from the QSO luminosity since

$$L_{Edd}/L_\odot \;=\; 3.3 \times 10^4 M_{BH}/M_\odot \qquad (12)$$

One then just needs to compare these to the properties of the host galaxy – which is where AO is important because spatial resolution is crucial to the success of this venture. From an astrophysical perspective, Fig. 5 shows that the near infrared is the best wavelength regime for studying QSO host galaxies. The QSO spectrum is dominated at short wavelengths by thermal emission from an accretion disk at $\sim 10^5\,\mathrm{K}$, and at long wavelengths by reprocessed emission from dust at 10^2–$10^3\,\mathrm{K}$, with a minimum in between at near infrared wavelengths. It is at such wavelengths that emission from the host galaxy, which is dominated by star light, reaches its maximum. An additional advantage of the near infrared regime is that one suffers less from the effects of extinction than optical; and at high redshift there is less bias towards only very recent star formation which is traced by the rest-frame UV continuum. In principle one could use HST/NICMOS, but AO on ground-based 8-m class

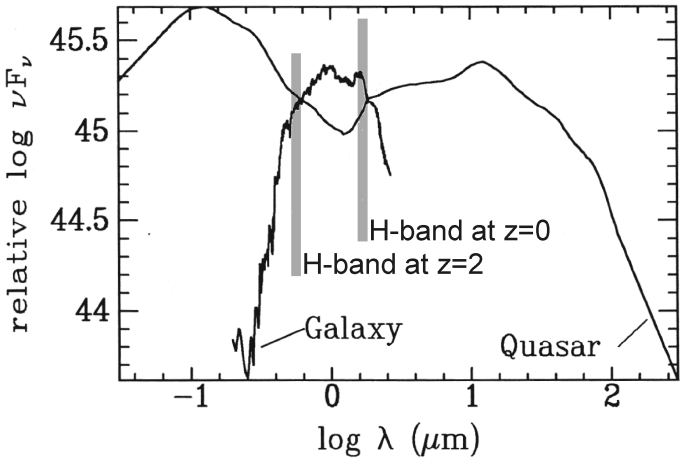

Fig. 5. Spectral energy distributions of a typical QSO and galaxy (arbitrarily scaled). The rest-frame location of the H-band for $z = 0$ and $z = 2$ spans the region where the host galaxy contrast is best. Adapted from McLeod & Rieke (1995).

telescopes can provide superior results due to the better spatial resolution, as well as the longer integrations and larger surveys that are needed (Hutchings, 2006).

3.3 QSOs and their Hosts at Low Redshift

The largest adaptive optics survey of QSO host galaxies to date was performed by Guyon et al. (2006) using the Gemini North and Subaru telescopes. They observed 32 nearby ($z < 0.3$) QSOs, mostly in the H-band ($1.6\,\mu$m), with a dynamic range of $> 10^4$ so that the host galaxies could be traced out to several arcseconds. PSF reference stars were observed for every target, using the same instrumental set-up. This is an important step, because to model the host galaxy, the bright QSO point source – including its extended wings – must be subtracted reasonably accurately. The scheme is outlined in some detail below, to demonstrate that this process is far from trivial, and requires subjective human input as well as an automated fitting routine. The authors modelled each host as sum of an exponential (appropriate for disks) or a de Vaucouleurs $r^{1/4}$ law (appropriate for spheroids). These can be quantified with a Sérsic profile using $n = 1$ or $n = 4$ respectively as

$$I(r) \;=\; I_e \exp(-b_n[(r/R_e)^{1/n} - 1]) \tag{13}$$

where R_e is the effective radius and b_n is a constant that varies with n to ensure that R_e encloses half the light. Each profile requires 4 parameters – brightness, size, orientation, and axis ratio – so that in Eq. 13 they replaced

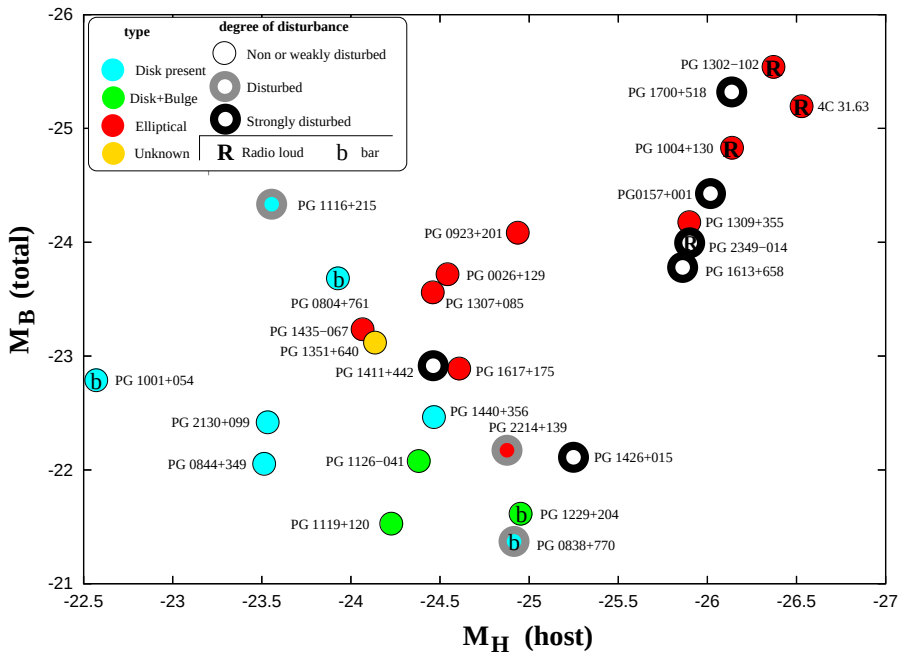

Fig. 6. Absolute B-mag of the QSOs plotted against absolute H-mag of the hosts for 27 objects. Different symbols and shades denote the morpholgoy of the host (disk or bulge or both) and the strength of any disturbances due to an interaction. From Guyon et al. (2006), courtesy of O. Guyon.

r with $f(r)$ for which

$$f(r) \;=\; r\sqrt{1+\sin^2(\theta-PA)\left[\frac{1}{(1-e)^2}-1\right]} \tag{14}$$

where PA is the orientation and e the elongation. In addition, the scale of the central point source is unknown, giving in total 9 free parameters. These were fit by minimising the residuals, which were quantified as

$$\chi^2 \;=\; \sum\left\{\left[image-(pointsource+host)\otimes PSF\right]/\sigma^2\right\} \tag{15}$$

This is an idealised scheme and cannot account for tidal tails or spiral arms. The residuals were therefore classified by eye, and a cross-check made to ensure that, for example, spiral arms only occur in disky hosts. In addition, the results for different bands were cross-checked manually.

Fig. 6 neatly summarises the three important results from this work.

(1) Lower luminosity hosts are mostly disks and high luminosity hosts are mostly ellipticals, but with a significant fraction of disturbed morphologies. This suggests that luminous hosts are the result of galaxy interactions or merger events.

(2) Disky hosts do not harbour really luminous QSOs. These are found in strongly disturbed or elliptical hosts. This suggests that luminous QSOs only occur in really major mergers which destroy the disk.
(3) Radio loud QSOs (which comprise ∼15% of the total, a typical fraction) are only found in the most luminous hosts. With the $M_{BH} - \sigma_*$ relation (and bearing in mind that the fundamental plane of early type galaxies implies σ is related to size and luminosity), this then suggests that the ratio of radio-quiet to radio-loud QSOs correlates with black hole size or perhaps black hole spin (see also Sikora et al., 2007).

One further result that Guyon et al. (2006) found concerned the amount of dust in the QSOs. This was quantified as the ratio between the reprocessed infrared luminosity L_{IR} and the direct optical luminosity L_{BB} (see Fig. 5). They found that elliptical hosts, which harboured the most luminous QSOs, also had the lowest ratios of L_{IR}/L_{BB} and hence were less obscured by dust. On the other hand, disky hosts typically had high ratios and hence more dust.

Taken together, these results strongly support current ideas about the evolutionary origin of QSOs, a scenario that was first put forward by Sanders et al. (1988) and has been supported observationally and theoretically by many others. It proposes that ULIRGs are formed by the merger of gas rich spiral galaxies. As this happens, gas falls to the centre where it can fuel both a starburst and an obscured AGN. Gradually the dust is cleared by radiation pressure and supernova, to reveal an optically bright QSO. When the fuel supply runs out, the QSO fades, leaving an old elliptical remnant. However, as we shall see later, this may not be the full story.

3.4 QSOs and their Hosts at High Redshift

At high redshift, this game is much more challenging, primarily because the QSO is often more luminous, but also because $(1+z)^4$ surface dimming makes the host much fainter. And because the angular size of the host is smaller at high redshift (at $z > 2$, $1'' \sim 8\,\mathrm{kpc}$), knowing the PSF becomes even more crucial. Thus, even detecting the host can often be difficult. For example, Croom et al. (2004) detected only 1 of 9 hosts at $z \sim 2$ using AO on Gemini North, and Falomo et al. (2005) detected only 1 of 3 hosts at $z \sim 2.5$ with AO on the VLT. Fortunately, even non-detections can yield useful luminosity limits. On the other hand, with an early AO system on a smaller telescope, Kuhlbrodt et al. (2005) detected all 3 hosts they observed. Although the host luminosities were consistent with the QSO/host luminosity relation, they were remarkably bright for their sizes. This implied a lower mass-to-light ratio, and hence a younger stellar population. The authors showed that if the age was 100 Myr at $z \sim 2.2$, then the hosts would fade onto the usual magnitude/size

relation by $z \sim 0$.

These results all have one aspect in common: they reduced the problem to estimating the host size and magnitude by assuming an elliptical profile. However, this assumption is not necessarily well justified. Using AO on the CFHT to observe a sample of nearby ($z < 0.6$) QSOs, Márquez et al. (2001) showed that there can be a bias in modelling the radial profile. They found that while elliptical hosts were always fit as ellipticals, disky hosts were also sometimes fit as ellipticals if the QSO was bright. Hutchings (2006) went so far as to state that "claims that all hosts at $z > 2$ are elliptical are suspicious." He has good reasons, and has shown that observations are strongly affected by dynamic range: bright inner bulges can be relatively easily seen and resolved at $0.1''$ scales, while fainter extended parts which may show signs of merging are much harder to detect. This concern was also shared by Canalizo et al. (2006) who reported deep HST/ACS observations of a QSO at $z \sim 0.2$ which has an elliptical host. Their data revealed faint shell structures, indicative of a merger event $\sim$1 Gyr in the past which would have triggered a burst of star formation.

These results highlight an on-going discussion about the stellar populations of QSO host galaxies: are they $\sim$10 Gyr old as one would expect for elliptical galaxies, or is there evidence for more recent star formation?

3.5 Are there Young Stars in the Centres of QSO Hosts?

This debate is covered in a recent review of QSOs and their host galaxies by Lacy (2006), but the two perspectives can be summarised as follows. In a carefully selected sample of luminous QSOs, Dunlop et al. (2003) found that all the hosts were quiescent ellipticals, perhaps with old populations. Supporting this, spectroscopic work by Nolan et al. (2001) found evolved stellar populations with ages $\sim$10 Gyr and only a small amount of recent star formation. In contrast, Kauffmann et al. (2003) found that the colours of the hosts of luminous QSOs were bluer than expected. This and other spectroscopic indicators implied significant star formation in the last 1–2 Gyr. Canalizo et al. (2006) re-examined the Dunlop sample, finding that in 13 of the 14 for which they obtained spectra, there was a population of stars making up at least 10% of the host's mass that had formed in the last 0.6–2.2 Gyr. But it is hard to understand how any event – even a major one such as a merger – 1 Gyr or more in the past could be the cause of current QSO activity.

In a twist on the second perspective, Canalizo et al. (2001) found spectroscopic evidence for very recent ($\sim$100 Myr) star formation in QSOs with a far-infrared excess. And adaptive optics observations of a few nearby QSOs

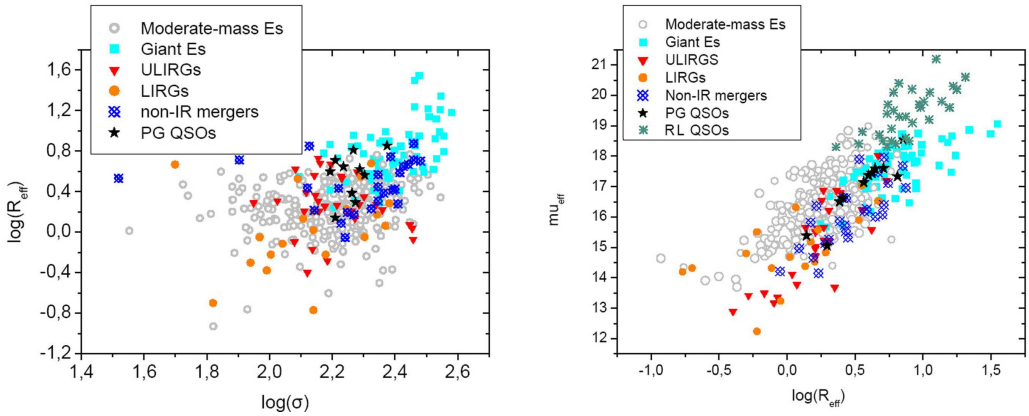

Fig. 7. Two projections of the fundamental plane for early type galaxies, for the effective radius ($R_{\rm eff}$), stellar dispersion (σ), and surface brightness ($mu_{\rm eff}$). Different symbols and shades denote the location of elliptical galaxies, ULIRGs, and QSOs. The IR-bright QSOs ('PG QSOs', black stars) occupy a similar region to ULIRGs (red triangles) and cluster ellipticals ('Moderate-mass Es', grey circles). The QSOs of Dunlop et al. (2003) ('RL QSOs', green asterisks) occupy the same region as giant ellipticals ('Giant Es', cyan squares). Adapted from Dasyra et al. (2007), courtesy of K. Dasyra.

have also revealed strong evidence for very recent star formation. Cresci et al. (2004) argued that the Paα emission in PG 1126-041 that was resolved on spatial scales of 100 pc was due to star formation. The inferred star formation rate of 13 $M_\odot\,{\rm yr}^{-1}$ could account for most of the object's far-infrared luminosity. Davies et al. (2004b) performed a detailed analysis of the unusual galaxy Mkn 231 using AO on the Keck telescope. They showed that the stellar profile and kinematics in the central 800 pc were consistent with a rotating disk; and in this region there was very intense (50–100 $M_\odot\,{\rm yr}^{-1}$) star formation which had created (1–5)$\times10^9\,M_\odot$ of stars in the last 10–100 Myr. Star formation within 1″ of the nucleus could account for about one third of the total luminosity of the galaxy and QSO combined. In Mkn 231 it is clear that the star formation has been triggered by the very recent merger event. But such a high star formation rate cannot be sustained, and Davies et al. (2004b) suggested that once it ceases and fades – on timescales of a few 100 Myr – Mkn 231 will probably look more like a typical AGN.

Some light can be shed on the issue of QSO hosts by work on stellar dynamics (Dasyra et al., 2006, 2007). While this was done without AO, it is certainly something which would benefit greatly from the technique. Building on earlier work, these authors measured the stellar dispersion in a sample of ULIRGs and QSOs, combining the results with data on the central surface brightness and the host effective radius. The remarkable result they found (see Fig. 7) is not only that ULIRGs lie on the same fundamental plane as intermediate mass elliptical galaxies, but that QSOs with infrared excess lie almost in the same region. This region, however, is significantly displaced from the locus

of radio-loud QSOs, which occupy a position more similar to that of giant elliptical galaxies. In addition, the infrared excess QSOs had $M_{BH} \sim 10^8\,M_\odot$, comparable to those of the ULIRGs, and hence relatively high Eddington efficiencies of order ∼0.25. These values were considerably different than those inferred for radio-loud QSOs, which have $M_{BH} \sim 5 \times 10^8$–$10^9\,M_\odot$ and hence Eddington efficiencies < 0.1. Thus, QSOs with infrared excess appear to be intrinsically different from radio-loud QSOs, suggesting that perhaps there might also be different causes for their nuclear activity.

Putting all these various results together, one might speculate that there are in fact two distinct paths to making a QSO. The first is to merge two gas-rich spiral galaxies, as in the standard evolutionary scenario. As has been modelled by many authors, this would lead to massive gas infall on short timescales, and hence both starburst and AGN activity. Signs of such events can remain for a very long time, and be observed as relic evidence of what has occured several Gyr in the past. However, detecting them does not necessarily mean that the major merger was directly responsible for all subsequent AGN fuelling. It is plausible that another event, perhaps accretion of new material from minor mergers or secular inflow, can also fuel the AGN and lead to renewed QSO activity several Gyr later. Certainly, there is still more to learn and understand about what different processes may lead to QSO activity and the role that the host galaxy plays in each. But it is also clear that adaptive optics has the potential to play an important part in this enterprise.

4 The Galactic Centre

At the other extreme, in terms of luminosity and distance, we turn to the Galactic Centre (GC) where there is a black hole of mass $4 \times 10^6\,M_\odot$ radiating at $< 10^{-10}$ of its Eddington luminosity. The proximity of this black hole (it is only 8 kpc distant) means that even the central parsec around it can be studied in incredible detail (Fig. 8), making it an obvious way-point on our quest to learn about AGN. Understanding why the massive black hole in the GC is accreting so little gas, and how this relates to other AGN where we do not have such a detailed view, must play an important part in piecing together the whole picture. As we shall see, adaptive optics has led to rapid developments in our knowledge of the Galactic Centre and its environment.

4.1 The Galactic Centre as a Quiescent AGN

At the current time, the GC can be considered a 'quiescent AGN'. The X-ray luminosity centered on Sgr A* is $\sim 2 \times 10^{33}\mathrm{erg\,s^{-1}}$ within the central 0.6″, im-

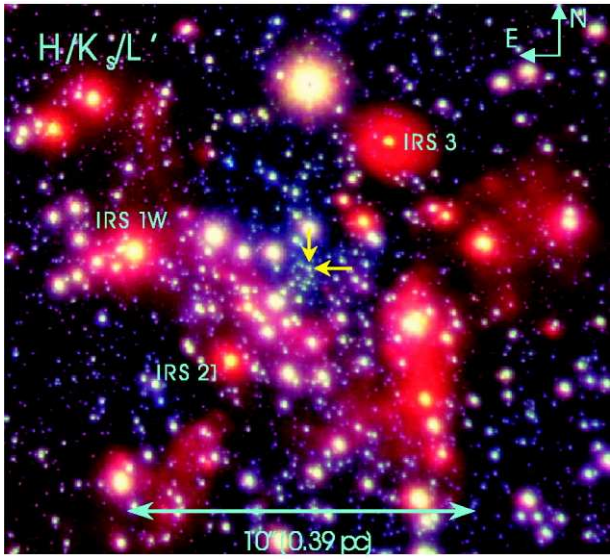

Fig. 8. Near infrared image of the Galactic Centre, showing the detail revealed by adaptive optics in the central half parsec. The guide star IRS 7 for the IR-WFS of NACO is top centre; the location of Sgr A* is marked. From Genzel et al. (2003a), courtesy of R. Genzel.

plying an accretion rate of $\sim 10^{-6}\,M_\odot\,\mathrm{yr}^{-1}$ on scales of 0.01 pc (Baganoff et al., 2003). And measurements of the linear polarisation at radio frequencies imply an accretion rate near the black hole's event horizon of $\lesssim 10^{-8}\,M_\odot\,\mathrm{yr}^{-1}$ (Bower et al., 2003). These are both very much less than the Eddington accretion rate for a $4 \times 10^6\,M_\odot$ black hole of $\sim 0.01/\eta\,M_\odot\,\mathrm{yr}^{-1}$ where $\eta \sim 0.1$ is an efficiency term. However, there is also evidence that only a few hundred years ago, Sgr A* was very much brighter. This comes from detailed X-ray images and spectra which show 3–200 keV emission from Sgr B2, a giant molecular cloud about 100 pc from Sgr A* (Koyama et al., 1996; Revnivtsev et al., 2004). The emission exhibits a 6.4 keV Kα line with a very large equivalent width, superposed on an absorbed continuum with strong emission above 20 keV. All these characteristics are supported by the interpretation that hard X-ray emission emitted by Sgr A* in the past has been Compton scattered and reprocessed by the Sgr B2 cloud. The distance between the clouds indicates that the outburst from Sgr A* must have happened 300–400 yr ago. And the luminosity of Sgr A* at that time would have been $\sim 10^{40}\,\mathrm{erg\,s}^{-1}$. While still only $10^{-5}\,L_{Edd}$, this is comparable to low luminosity AGN which have luminosities in the range 10^{-3}–$10^{-6}\,L_{Edd}$ (Ho, 1999). We will re-visit this issue in Section 4.3, where we look at why Sgr A* is so faint, a property that can be considered an advantage since it allows us to study the environment close around the black hole without being dazzled by its glare.

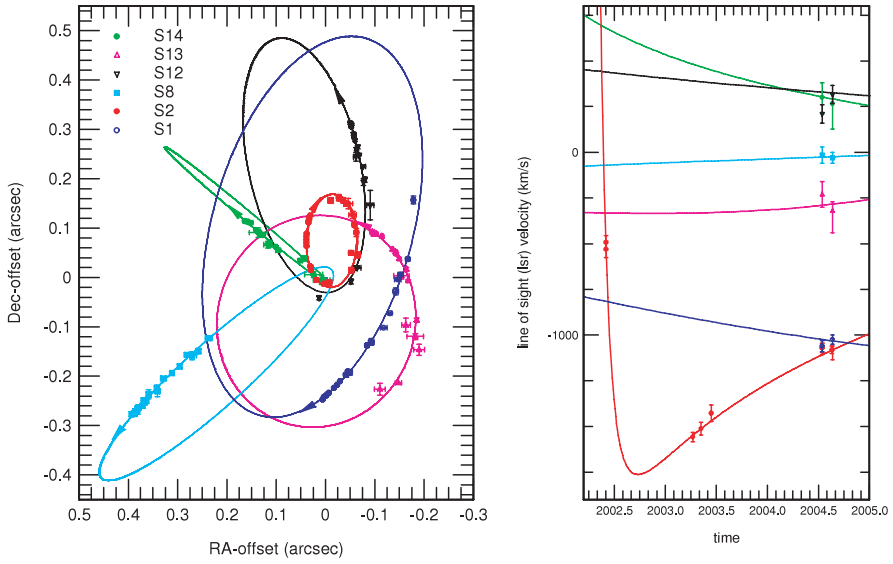

Fig. 9. Proper and Radial motions of 6 S stars in the GC, together with their orbital solutions. From Eisenhauer et al. (2005), courtesy of F. Eisenhauer.

4.2 Stellar Motions

At optical wavelengths, the GC cannot be seen as it is hidden behind $A_V \sim 30$ mag of extinction. Fortunately, the fact that this corresponds to only $A_K \sim 3$ mag at near infrared wavelengths, and that there is an incredibly bright $K \sim 6$ mag star, IRS 7, less than $6''$ from Sgr A* (see Fig. 8) means that the GC is ideally suited to adaptive optics with an infrared wavefront sensor. Over the last decade, adaptive optics – with visible WFS, infrared WFS, and LGS – has driven the huge advances made in the GC, much of which is related to the stars: their number density, their spectral types, and their motions.

It is tracking of stellar proper motions that is perhaps one of the most remarkable facets of GC adaptive optics research. A 15 year (and continuing) campaign has led to measurements circumscribing a complete orbit of the S2 star, the projected size of which is only $0.2''$. Combining the proper motion with radial velocity measurements has allowed a fully constrained orbital solution – including a geometric distance to the GC – to be determined (Eisenhauer et al., 2005). These data confirm that the closest approach of S2 to Sgr A* was only 17 light-hours, at which point it had a velocity of $8000\,\mathrm{km\,s^{-1}}$; and that its orbit has a 15.2 yr period and a semi-major axis of $0.12''$. The latter two measurements yield an estimation of the central mass that is contained within a few light hours around Sgr A* using Kepler's 3^{rd} law:

$$\left(\frac{P}{2\pi}\right)^2 = \frac{a^3}{G(M+m)} \tag{16}$$

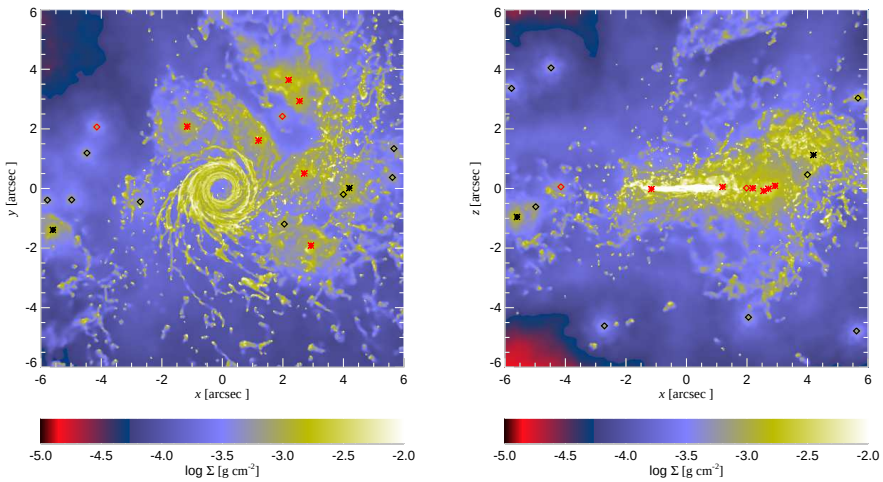

Fig. 10. End state of the simulation from Cuadra et al. (2006) showing the column density of gas for 2 projections. The positions of the stars are marked by asterisks (for slow winds) or diamonds (for fast winds). It can be seen that a hot gas phase fills the central cavity and a cold gas phase has settled into a disk. Courtesy of J. Cuadra.

It is fascinating to realise that one can still do modern research using 400-year-old physics – as long as one has access to state-of-the-art technology. This technology has now made it possible to derive useful orbital solutions for more than 15 stars (Ghez et al., 2005; Trippe et al., 2006), of which 6 are shown in Fig. 9.

4.3 Why is SgrA so Faint?*

It has already been mentioned that Sgr A* is remarkably faint. This ought to be unexpected, since we know that on scales of 10 pc, the gas inflow rate is of order $10^{-2}\,M_\odot\,\mathrm{yr}^{-1}$ (Mezger et al., 1996). This is sufficient material to fuel a Seyfert nucleus. Yet the actual accretion rate onto the black hole is 6 orders of magnitude less. The reason, as proposed by Ozernoy & Genzel (1996), is that inflow is hindered by the outflow and angular momentum of the winds from massive young stars that were formed in a recent starburst 5–7 Myr ago (Paumard et al., 2006). This scenario has been modelled in detail by Cuadra et al. (2006). They included both the fast young stellar winds with velocities of $700\,\mathrm{km\,s}^{-1}$ (Ozernoy et al., 1997) and the slower winds of $\sim 200\,\mathrm{km\,s}^{-1}$ (Paumard et al., 2001), with a total mass-loss rate of $\sim 10^{-3}\,M_\odot\,\mathrm{yr}^{-1}$. They also accounted for the angular momentum of the stars by putting them on orbits at $R \sim 0.5$ pc resembling those that have been observed (Genzel et al., 2003a; Paumard et al., 2006). The gas had a two-phase structure. While much of it flowed outwards, the gas that remained within the simulation volume consisted of a hot phase filling the central cavity and a cold phase that con-

densed into filaments and fell inwards, settling onto a disk on spatial scales of about 0.05 pc (Fig. 10). The simulation yielded two distinct ways in which the black hole could be fuelled. The average accretion rate – provided by the hot phase – was only $\sim 3 \times 10^{-6}\, M_\odot\, \mathrm{yr}^{-1}$, comparable to that observed on similar scales of 0.01 pc. In general, higher accretion rates were hindered by the angular momentum of the gas. But superimposed on the base level was a very significant variability caused by the cold phase as distinct clumps were sporadically accreted. More recent simulations (Cuadra et al., 2008) using stellar properties specific to individual stars observed in the GC suggest that there are not enough slow winds to form a conspicuous cold disk, but that occasional cold clumps do nevertheless generate some variability in the accretion rate. The behaviour in these simulations is reasonably consistent with what has been observed, and also has many features in common with models of Seyfert galaxies which will be discussed in Section 5.

4.4 Infrared and X-ray Flares

One of the most exciting discoveries in the GC during the last few years is that of near infrared flares from Sgr A* (Genzel et al., 2003b), an example of which can be seen in Fig. 11. These occur about twice a day and appear to last for order 1 hr. The substructure in the light curve on a time scale of 17 mins has been interpreted in terms of matter on the last stable orbit, implying that the black hole has a spin of $a = 0.5$. In order to understand the physics behind these events, there have been a number of attempts to obtain spectral information of the flares. Gillessen et al. (2006) report that the near infrared spectral slope changes with flare brightness; Eckart et al. (2006) present coordinated (and sometimes simultaneous) observations across many wavelength regimes (0.7 cm, 0.89 mm, 1.7–3.8 μm, and 2–8 keV). The general consensus of these efforts is an understanding that the flare is related to, but not directly produced by, the radiatively inefficient accretion flow (RIAF) that is believed to produce the peak of the submillimetre emission. The RIAF model underpredicts the 2 μm flux, which instead originates from electrons that are locally and transiently heated. As this compact source orbits the black hole, significant variability ensues from a combination of synchrotron cooling and orbital dynamics, both of which operate on a timescale of ~ 20 mins. In this model, the high Lorentz factor of the electrons, $\gamma \sim 10^3$ means that the X-ray emission is most likely to arise from inverse Compton scattering.

A daring way to observationally constrain such models has been proposed for GRAVITY, a 4-beam combiner for VLTI that is currently in its design phase (Eisenhauer et al., 2008). The two main capabilities of GRAVITY will be phase-referenced imaging over an 80 mas field, and narrow angle astrometry to 10 μas accuracy. The proposal put forward by Paumard et al. (2008) utilises

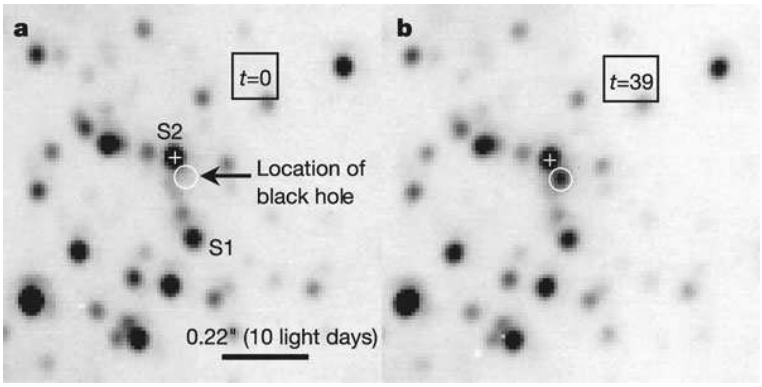

Fig. 11. H-band images of the Galactic Centre showing the location of Sgr A* near the centre. A flare from around the black hole has been detected in the righthand frame. From Genzel et al. (2003b), courtesy of R. Genzel.

both of these. The former will provide images of stars very close to Sgr A*, and hence yield proper motions of these stars. The velocities of these stars are expected to be huge, so that within a relatively short time, one should be able to measure orbit precession due to both the extended mass distribution and also relativistic effects. The astrometric capability will enable the centroid of the flares to be pinpointed to an accuracy corresponding to the Schwarzschild radius R_S with less than 1 min integration time. Thus it will be possible to track the motion of the flare centroid as it evolves; and, if each flare traces the same orbit, co-add observations from different flares to increase the signal-to-noise. Relativistic ray tracing indicates that if the flare does indeed originate from a compact spot of transiently heated electrons, then such methods will be able to constrain the geometry and physical conditions prevailing at distance of a few R_S around the Galactic Centre's black hole.

5 Nearby Active Galactic Nuclei

Nearby galaxies – at distances of a few to a few tens of Mpc – present an opportunity to observe the AGN phenomenon in a larger number of objects on scales suited to studying some of their major structures. These AGN are almost exclusively Seyfert galaxies, which are less luminous then QSOs but are believed to fit into the same unification scheme. In such galaxies, AO allows us to reach spatial resolutions corresponding to 1–50 pc. One is therefore able to resolve the circumnuclear region of the host galaxy, the Narrow Line Region, the obscuring molecular torus and the nuclear region of the host galaxy, and in some cases the sphere of influence of the central supermassive black hole.

The Seyfert galaxy NGC 1068 at a distance of 14 Mpc is perhaps an obvious choice, not only due to its proximity, but because it is considered to be 'prototypical' and has one of the brightest nuclei. It has been the subject of many

studies, even from the early days of adaptive optics (Rouan et al., 1998, 2004; Marco & Alloin, 2000; Gratadour et al., 2003, 2005, 2006; Mueller Sanchez et al., 2008) and interferometry (Jaffe et al., 2004). A few Seyfert galaxies lie nearer still. In particular, at distances of only ∼4 Mpc – where 60 mas, the K-band diffraction limit of an 8-m telescope, corresponds to 1 pc – are the Circinus Galaxy and Centaurus A. Wavefront sensing on these objects is more challenging, and it has only been possible relatively recently to observe and study them with AO (Prieto et al., 2004; Mueller Sanchez et al., 2006; Neumayer et al., 2007) or interferometry (Tristram et al., 2007; Meisenheimer et al., 2007). Adaptive optics systems have also been pointed towards a few other AGN, including Mkn 231 (Lai et al., 1998; Davies et al., 2004b), M 81 (Davidge & Courteau, 1999), NGC 6240 (Bogdanović et al., 2003; Max et al., 2005; Pollack et al., 2007), NGC 7469 (Davies et al., 2004a), NGC 1097 (Prieto et al., 2005), and NGC 3227 (Davies et al., 2006).

A few of these objects were also included in a sample of nearby AGN observed by Hicks & Malkan (2008) to study molecular gas dynamics with an aim to estimating their black hole masses. A number were also included in the work that makes up much of what is presented in this Section, based on observations with the adaptive optics near infrared integral field spectrometer SINFONI (Eisenhauer et al., 2003; Bonnet et al., 2004). This sample comprises 9 galaxies which were observed using the AGN itself as the AO wavefront reference (Davies et al., 2007; Hicks et al., 2008). The open questions that we will address with the data here aim to (1) measure the black hole mass using spatially resolved stellar kinematics; (2) derive the properties of the molecular gas, and understand its relation to the torus; and (3) determine the extent and history of star formation, and its relation to the AGN and torus.

5.1 Black Hole Masses

There are many ways to measure black hole masses depending on how far away the AGN is and hence what spatial scales can be resolved. For nearby AGN, stellar or gas kinematics represent a good option. Gas kinematics are often easier to model since gas cools into a thin rotating disk on short timescales, and can usually be modelled as such. However, gas can also be strongly influenced by inflows and outflows. For that reason, stellar kinematics are preferred, although the modelling is more complex. In either case, an important issue is that the radius of influence of the black hole R_h is resolved. This is defined as the radius within which the black hole mass, rather than the stellar mass, dominates the gravitational potential, and is (Ferrarese & Ford, 2005)

$$R_h \sim \frac{GM_{BH}}{\sigma_*^2} \sim 11.2 \left(\frac{M_{BH}}{10^8\, M_\odot}\right) \left(\frac{\sigma_*}{200\, km\, s^{-1}}\right)^{-2} pc \qquad (17)$$

where σ_* is the velocity dispersion of the stellar spheroid around the black hole. On the other hand, we know from the M_{BH}-σ_* relation that (Tremaine et al., 2002)

$$M_{BH} \ = 1.35 \times 10^8 \left(\frac{\sigma_*}{200\, km\, s^{-1}} \right)^{4.02} \ M_\odot \tag{18}$$

And putting Eqs. 17 and 18 together one gets, to zero order, an estimate of R_h which depends only on M_{BH}

$$R_h \ \sim \ \left(\frac{M_{BH}}{10^6\, M_\odot} \right)^{0.5} \ pc \tag{19}$$

Thus, with adaptive optics on an 8-m telescope, one can resolve R_h in a typical Seyfert galaxy harbouring a $10^7\,\mathrm{M}_\odot$ black hole out to a distance of $\sim 20\,\mathrm{Mpc}$.

Many black hole mass estimates have been derived from the line-of-sight velocity distributions (LOSVDs) extracted from long-slit data along particular axes. In contrast, integral field data maps the complete spatial distribution of the LOSVDs, and so is more robust. The reason, explained clearly by Cappellari et al. (2004a), is that long-slit data may miss some orbits if the (localised) regions of high projected surface brightness do not happen to fall within the slit. As a result, a model derived using long-slit data may be significantly different from that found from integral field data.

The LOSVD itself is usually characterised in terms of Gauss-Hermite functions. These include the velocity V and dispersion σ of a simple Gaussian, as well as the 3^{rd} and 4^{th} Hermite terms which quantify respectively the asymmetry and flatness of the profile (see Bender et al., 1994, for a more complete description of these). The LOSVDs are extracted by deconvolving the galaxy spectrum using spectra of local stellar templates. Typically several are employed to reduce problems of template mismatch due to the varying depths of the different absorption features. There are two commonly used methods: division of the galaxy spectrum by the template in the Fourier domain; or direct convolution of a function with the template to match the galaxy spectrum. Now that computer power is not a limiting issue, the latter method is increasingly used, and it leads to either a full non-parametric LOSVD or to a parameterisation at the desired level of detail. A discussion of this process, including a detailed analysis of one particular method, is given by Cappellari & Emsellem (2004b). Finally, once the LOSVDs have been extracted, one can begin to model them.

The kinematics of stellar spheroids are modelled using an orbit superposition method developed originally by Schwarzschild (1979), and extended by Cretton et al. (1999) to the more general three integral axisymmetric models that

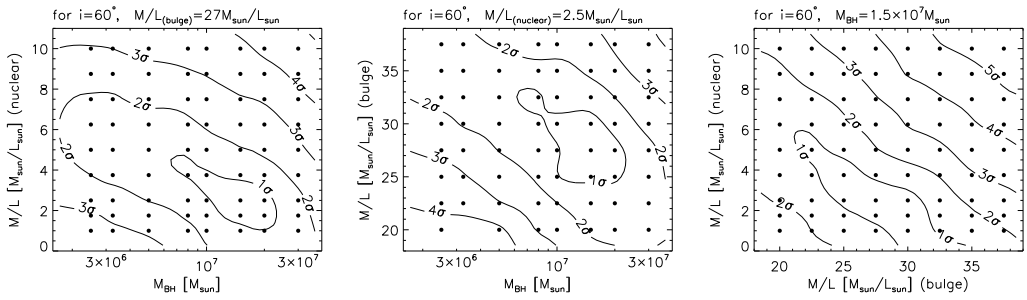

Fig. 12. Slices through the χ^2 landscape for the Schwarzschild modelling performed on NGC 3227, showing how the 3 parameters are correlated. Left: at a fixed $M/L_{bulge} = 27\,M_\odot/L_\odot$. Centre: at a fixed $M/L_{nuclear} = 2.5\,M_\odot/L_\odot$. Right: at a fixed $M_{BH} = 1.5 \times 1{-}7\,M_\odot$. From Davies et al. (2006).

are commonly used now. At the start of each step one specifies the black hole mass and the mass-to-light ratio of the stars, and uses those together with the observed luminosity distribution to define the gravitational potential. One then follows the equations of motion to build up a library of several thousand pro- and retro-grade orbits distributed through parameter space (comprising energy, angular momentum, and a more abstruse 'third integral'). A linear non-negative combination of orbits is then found that matches the luminosity profile and reproduces as closely as possible the observed LOSVDs. One can then repeat the process using different input parameters: black hole mass, mass-to-light ratio, inclination, and so on. There are inevitably details which need to be carefully considered (see, for example, Thomas et al., 2004, and references therein), but the final result is that, via a χ^2 minimisation, one can find the optimal parameters as well as their associated uncertainties.

The example of NGC 3227 (Davies et al., 2006) demonstrates several important issues that should be borne in mind. For this object, two stellar components were included, representing the bulge of older stars and a thick nuclear disk of younger stars. The resulting χ^2 landscapes for the three parameters (M_{BH}, M/L_{bulge}, and $M/L_{nuclear}$) is shown in Fig. 12. Firstly, each pair of parameters are apparently correlated. This is because the mass on small spatial scales can either be in a black hole or in the nuclear disk; and on slightly larger scales, the mass can be distributed either in the disk or bulge. Thus, the parameters are not entirely independent. Secondly, it suggests that the derived black hole mass should instead be considered as the unresolved central mass, which may include a compact stellar component. Some work along these lines has been pursued by Ferrarese et al. (2006), but the topic remains highly controversial. Thirdly, consistency checks are important. The NGC 3227 model yielded $M/L_{bulge} = 27.5\,M_\odot/L_\odot$, within the range 25–35 $M_\odot/L_\odot$ expected for bulges of spiral galaxies (Förster Schreiber et al., 2003). On the other hand, it suggested that $M/L_{nuclear} = 2.5\,M_\odot/L_\odot$, a factor of 5 larger than that derived from modelling the starburst using evolutionary synthesis code. The reason is that the mass of the thick nuclear disk includes a substantial contribution

from molecular gas, so that its effective ratio is $M/L_{nuclear} = 1\text{–}5\,M_{\odot}/L_{\odot}$. Thus the model result is consistent with expectations. It is such consistency checks that can give one confidence that the derived black hole mass – in this case $1.5 \times 10^7\,\mathrm{M}_{\odot}$ – is reliable.

5.2 Obscuring Molecular Gas

To understand how the molecular gas seen in the SINFONI data is related to the obscuring molecular torus, one first needs to clear one's mind of any preconcieved ideas about how the torus should look. Instead, we must think only of the minimum global criteria that are necessary for a structure to be described as the torus. These are that it (1) consists of molecular gas and dust; (2) is compact, with a size no more than several tens of parsecs; (3) is optically thick, so that it obscures the AGN when edge-on; (4) is vertically extended, by several parsecs, so as to provide collimation for ionisation cones. As we summarise briefly below, Hicks et al. (2008) argues that these criteria are indeed fulfilled.

The near infrared molecular gas tracer is the 1-0 S(1) ro-vibrational line of H_2, and arises in gas that is heated to temperatures of $(1\text{–}2)\times10^3\,\mathrm{K}$. Since this can only occur at the edges of clouds, the line traces only $\sim 10^{-6}$ of the total gas mass, and on small scales can be strongly influenced by the local environment (e.g. proximity of young stars, supernova remnants, etc.). Nevertheless, on large scales it is believed to trace reasonably well the distribution of molecular gas – and its presence indicates that there is certainly molecular gas there, as one would expect for the torus. The size scale can be found from the half-width at half maximum of the radially averaged profiles of the line. These are typically less than 50 pc, and in many cases much less. The optical depth, or equivalently column density, is harder to derive because the line traces such a small fraction of the total gas mass. However, it can be estimated from the dynamical mass (based on the observed velocity and dispersion), assuming an appropriate gas mass fraction. Hicks et al. (2008) argue that 10% is a conservative fraction, and even this implies a column density of more than $10^{23}\,\mathrm{cm}^{-2}$. Given that extinction A_V is related to the gas column density n_H as $A_V \sim n_H(\mathrm{cm}^{-2})/10^{21}$, this is more than enough to obscure the AGN even at near infrared wavelengths. Evidence for a vertically extended geometry comes from the large $50\text{–}100\,\mathrm{km\,s}^{-1}$ velocity dispersion of the gas. The 1-0 S(1) line emission is strongest if it is excited in shocks with speeds of $20\text{–}40\,\mathrm{km\,s}^{-1}$. Higher velocities would dissociate the H_2 molecules and reduce the 1-0 S(1) line intensity. However, high dispersions can be produced if there are bulk motions – such as dense clouds moving at high speeds, as observed in Orion (Tedds et al., 1999). There the 1-0 S(1) emission originates in oblique shocks on the sides of the clouds, and the width of the line, when integrated over

the cloud, yields a measure of the speed of the cloud. A very broad 1-0 S(1) line is therefore an indication that there are oblique shocks occurring on many clouds which are moving in different directions, suggesting that the molecular gas seen close around AGN is vertically extended.

Thus, it is fair to conclude that adaptive optics observations of nearby AGN do resolve the global structure of the torus. In Section 5.4 we shall see how these large scale properties can be reconciled with the small scale structures inferred from interferometric observations.

5.3 Nuclear Star Formation

Over the last decade, there has been increasing evidence that starbursts do occur close to a majority of AGN. This has led to a framework in which the fundamental questions concern the extent to which AGN and nuclear star formation might impact each other via their feedback mechanisms. Since this is closely related to how energetically significant starbursts are around AGN, considerable effort has been devoted to studying starbursts in local Seyfert nuclei. The largest of these studies (Cid Fernandes et al., 2004) made use of empirical population synthesis, finding unambiguous evidence for recent (<1Gyr) star formation within a few hundred parsecs of the nuclei in about 40% of Seyfert 2 nuclei. However, to address whether there might a causal relationship, one needs to probe the star formation in more detail. This is where adaptive optics plays a crucial role, not only providing higher spatial resolution, but doing so in Seyfert 1 nuclei where historically the glare from the AGN itself has overwhelmed any starburst signature.

Such work with AO was the focus of a study by Davies et al. (2007) on the sample of AGN observed with SINFONI. The authors first explain how to separate the stellar and non-stellar contributions to the near-infrared continuum using the equivalent width of stellar absorption features. They go on to show that one can in principle estimate the stellar bolometric luminosity to within a factor of 3 without knowing anything about the star formation history, although they do use several independent diagnostics to better constrain the star formation age. Their findings are that (1) the nuclear star forming regions are spatially resolved, with half-widths of 50 pc or less; (2) there has been recent star formation within the last few hundred Myr; (3) the star formation is no longer active, implying that nuclear starbursts are short-lived phenomena. The way in which this star formation might be linked to both the torus and to the AGN itself is the topic of the following two sections.

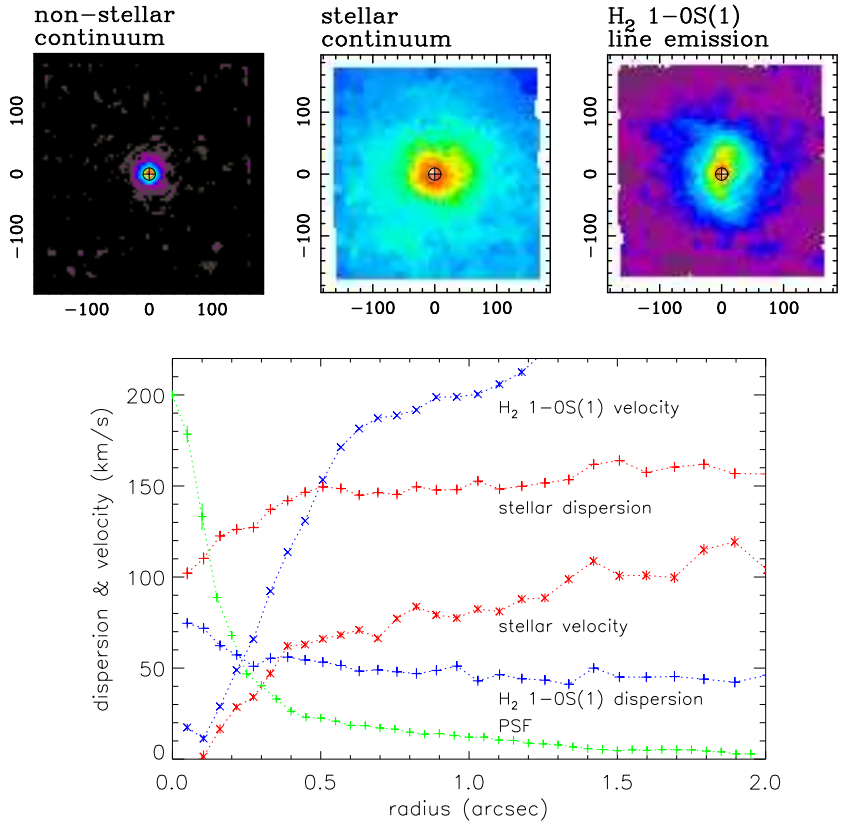

Fig. 13. Distribution (top) and azimuthally averaged kinematics (bottom) for the stars and molecular gas in NGC 1097. Axes are marked in parsecs (top) and arcsec (bottom). For NGC 1097, 1″ corresponds to 80 pc. Adapted from Davies et al. (2007).

5.4 The Star-Forming Torus

In the previous two sections, we have seen that both the gas and stars in the nucleus have half-widths less than about 50 pc. Although not conclusive in itself, this suggests that the stars and gas (and hence the torus) may be related. However, it is the kinematics that are needed to decide whether they actually occupy the same volume. NGC 1097 (Fig. 13) is a clear example where this appears to be the case. The rotation curves of the gas and stars are completely different at radii $> 0.5''$. When interpreted with the dispersion, they indicate that the stars are in a spheroidal structure dominated by random motions (i.e. the bulge) whereas the gas is in a thin disk supported by ordered rotation. But at radii $< 0.5''$, the gas rotation curve drops rapidly and quickly becomes very similar to that of the stars. Similarly, the dispersion of the stars drops while that of the gas increases. Thus the stellar and gas kinematics become remarkably similar at small radii. The only possible explanation is that in the nucleus, the gas and stars are physically mixed.

If one draws all the various threads together, one is led to the intriguing conclusion that starbursts close around AGN are intense and short-lived events that recur episodically. The hypothesis of Davies et al. (2006, 2007) is that gas accumulates in the central 100 pc region, either gradually or by stochastic accretion onto these scales of a number of giant molecular clouds. At first stars cannot form, because the interstellar medium is too turbulent; but eventually as the gas density increases, star formation does ensue. This is simply a statement of the Toomre criterion

$$Q \;=\; \frac{\sigma\kappa}{\pi G\Sigma} \tag{20}$$

where the relevant parameters here are the dispersion σ and mass surface density Σ. The value of Q is a balance between high mass density facilitating star formation, and turbulence hindering it. Only when $Q < 1$ can star formation take place. The global Schmidt law formulated by Kennicutt (1998) states

$$\Sigma_{SFR} \;\propto\; \Sigma_{gas}^{1.4} \tag{21}$$

so that when star formation does occur, the gas mass density is so high that star formation is extremely rapid and efficient. This will mean that the starburst is inevitably short-lived. And the combined effects of radiation pressure, and later turbulence induced by supernovae, will also help to shut off the star formation. The starburst will fade relatively quickly, and the region will then remain dormant until the gas is replenished by further inflow to the central 100 pc. While this scenario may sound plausible, it still needs to be verified theoretically, and much work also remains on understanding in detail how such a scheme might work.

5.5 The AGN-Starburst Connection

One consequence of the $M_{BH} - \sigma_*$ relation, that black holes and bulges grow in tandem, is that understanding how feedback moderates star formation and black hole growth has become an increasingly relevant issue. We have already enountered this in Section 3.5, and it appears in many other arenas. One of these concerns how early type galaxies evolve from the 'blue cloud' to the 'red sequence' – regions on plots of the stellar mass against colour. This evolutionary path has been studied by many authors, notably Schawinski et al. (2007). These authors took a sample of 16000 early type galaxies from the Sloan Digitised Sky Survey, and measured their AGN properties (via emission lines) and star formation history (via absorption features and multi-colour photometry). They could very clearly separate the star forming galaxies which inhabited the 'blue cloud' from the quiescent galaxies which occupied the 'red sequence'.

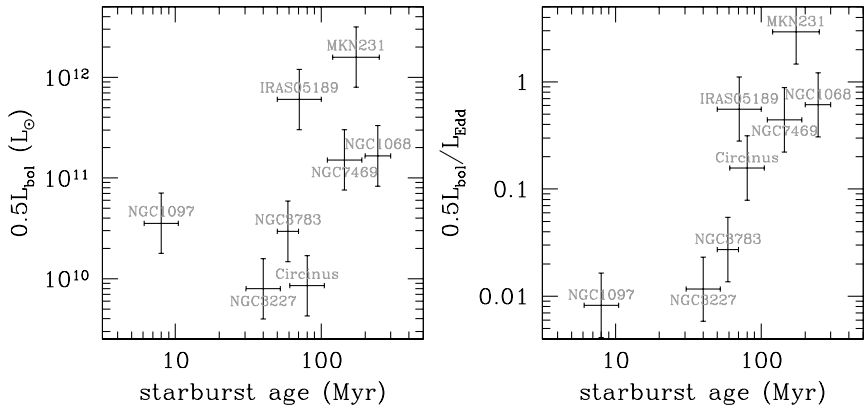

Fig. 14. Graphs showing how the luminosity of an AGN (left) or its accretion rate (right) might be related to the age of the most recent episode of star formation. From Davies et al. (2007).

But they also found evidence of an evolutionary sequence in which the Seyfert galaxies occupying the 'green valley' in between exhibited characteristics of intermediate age star formation. Their analysis showed that the peak AGN phase occurs roughly 0.5 Gyr after the starburst, and they suggested that this was due to suppression of the star formation (on large scales) by the AGN feedback.

A rather different conclusion – that the starburst (on very small scales) has a considerable impact on the AGN fuelling – was reached by Davies et al. (2007) from the AO data discussed in Section 5.3. This analysis produced a qualitatively similar result, shown in Fig. 14, that the AGN appears to be switched on 50–100 Myr after the starburst has begun. However, it was interpreted as a delay of the AGN fuelling induced by the starburst. A crucial aspect of this may be the stellar ejecta; and in particular not just the mass loss rate but the ejection speed. In Section 4.3 we saw that in the Galactic Centre, winds from OB stars are hindering gas accretion onto the black hole. Similarly, it is likely that supernovae, each of which may eject $5\,M_\odot$ of mass at $5000\,\mathrm{km\,s^{-1}}$, will also do so. It is known that starbursts often lead to superwinds in which a significant fraction of the interstellar medium is ejected – perhaps the best known example is M 82. For a starburst of short duration, the supernova rate peaks at ages of 10–50 Myr. Fig. 14 shows that this is the period when the AGN are in a low luminosity phase, supporting the idea that supernovae hinder accretion. On the other hand, stars of 1–8 $M_\odot$ reach the end of their main sequence lives after $\sim$ 50 Myr, and evolve into thermally pulsing asymptotic giant branch (AGB) stars. Their winds, which have much slower speeds of 10–30 $\mathrm{km\,s^{-1}}$, will remain bound. And because they are still associated with significant mass loss, could, in principle, provide sufficient fuel to power a Seyfert nucleus.

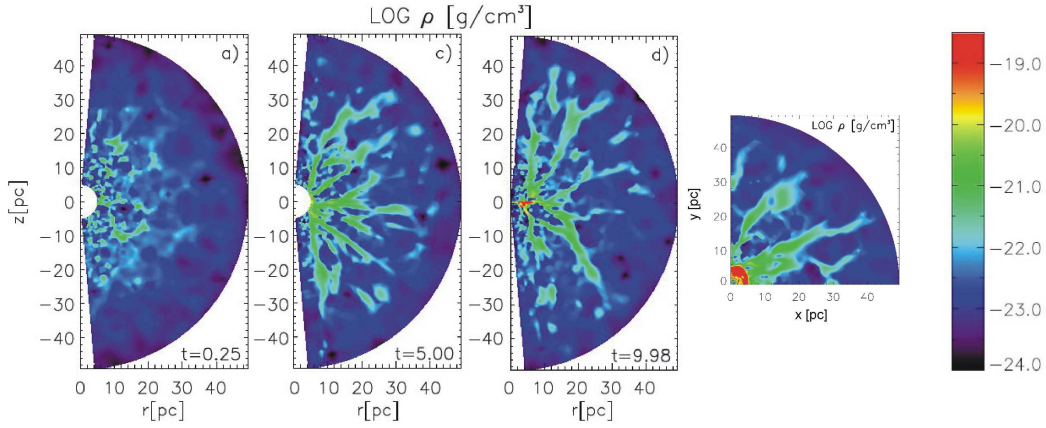

Fig. 15. Hydrodynamical simulations of the impact of stellar evolution on the gas around an AGN. Left three panels: gas density in meridional plane at the start and after 5 and 10 orbits. Right panel: gas density in the equatorial plane after 10 orbits. The filamentary structure and compact turbulent disk are clearly seen. Adapted from Schartmann (2007), courtesy of M. Schartmann.

Intriguingly, hydrodynamical simulations of the impact of stellar evolution on gas in the central 50 pc of AGN have led Schartmann (2007) to a remarkably similar conclusion to that above. He found that supernovae can blow low density gas away, leaving long dense filaments (Fig. 15). The interplay between these filaments and the slower stellar ejecta lead to inward accretion to form a central turbulent disk. There are 3 insights that one can immediately draw from this work. The first is that a starburst does indeed have a dramatic impact on the nuclear region, and that gas ejected in slow winds can be accreted along filaments. Secondly, there is a hint that the torus may actually have substructure: a larger scale diffuse part consisting of long filaments, and a small scale dense turbulent disk. It would be the former structure that the AO data have found; and the latter that shows up most prominently in interferometric observations of AGN. Finally, the processes operating in this simulation of AGN are basically the same as those seen in the Galactic Centre (Fig. 10). The main difference is that of spatial scale which may, as suggested by Thompson et al. (2005), be related to the mass of the central black hole. With hindsight, the similarities should perhaps not be surprising, since the physics in both environments concerns the impact of stellar winds on the ISM and inward accretion. It is a salutary lesson that there is much to be learnt by adopting a broad perspective.

6 Outlook

In these lectures we have taken a brief look at how adaptive optics works, and how it has led to new insights in studies of AGN on many spatial scales. At

high redshift, AO enables one to resolve the host galaxy of AGN on kpc scales. In the Galactic Centre, it opens up a detailed view on the sub-parsec scale. And in nearby galaxies, it yields a resolution comparable to the size scale of a number of the structures which make up an AGN.

The next few years will be a very exciting time, as new advanced AO systems become available to the community on several different large telescopes. These include the multi-conjugate laser guide star system on Gemini South, which will use 5 LGS and 3 NGS to control 3 DMs, and provide diffraction limited resolution at 1-2.5 μm across a field of view of more than 1 arcmin. LINC-NIRVANA on the Large Binocular Telescope will use multiple NGS to flatten the wavefront so that the beams from the two mirrors can be combined interferometrically, yielding images with a resolution equivalent to that of a 23-m telescope. MUSE on the Very Large Telescope will make use of the multiple laser guide stars available with the Adaptive Optics Facility to provide either enhanced resolution over 1 arcmin, or diffraction limited resolution over a smaller field – both at optical wavelengths. These systems will open up many possibilities for studying AGN across all spatial scales. The progress that can be made will be limited only by the imagination of those who wish to use them.

Acknowledgements

It is a pleasure to thank all those who have generously contributed figures, and to those who have patiently commented on the text. I would also like to thank the referee for a number of helpful suggestions. Finally, I thank the school organisers for inviting me to give these lectures.

References

Baganoff F., et al., 2003, ApJ, 591, 891
Beckers J., 1993, ARA&A, 31, 13
Bender R., Saglia R., Gerhard O., 1994, MNRAS, 269, 785
Bogdanović T., Ge J., Max C., Raschke L., 2003, AJ, 126, 2299
Bonnet H., et al., 2004, The ESO Messenger, 117, 17
Bower G., Wright M., Flacke H., Backer D., 2003, ApJ, 588, 331
Canalizo G., Stockton A., 2001, ApJ, 555, 719
Canalizo G., Stockton A., Brotherton M., Lacy M., 2006, NewAR, 50, 650
Cappellari M., et al., 2004, in *Carnegie Observatories Astrophysics Series, Vol. 1: Coevolution of Black Holes and Galaxies* ed. Ho L.
Cappellari M., Emsellem E., 2004, PASP, 116, 138

Cid Fernandes R., Gu Q., Melnick J., Terlevich E., Terlevich R., Kunth D., Rodrigues Lacerda R., Joguet B¿, 2004, MNRAS, 355, 273
Cresci G., Maiolino R., Marconi A., Mannucci F., Granato G., 2004, A&A, 423, L13
Cresci G., Davies R., Baker A., Mannucci F., Lehnert M., Totani T., Minowa Y., 2006, A&A, 458, 385
Cretton N., de Zeeuw T., van der Marel R., Rix H.-W., 1999, ApJS, 124, 383
Croom S., Schade D., Boyle B., Shanks T., Miller L., Smith R., 2004, ApJ, 606, 126
Cuadra J., Nayakshin S., Springel V., Di Matteo T., 2006, MNRAS, 366, 358
Cuadra J., Nayakshin S., Martins F., 2008, MNRAS, 383, 458
Dasyra K., et al., 2006, ApJ, 651, 836
Dasyra K., et al., 2007, ApJ, 657, 102
Davidge T., Courteau S., 1999, AJ, 117, 2781
Davies R., Eckart A., Hackenberg W., Ott T., Butler D., Kasper M., Quirrenbach A., 2000, ExA, 10, 103
Davies R., Tacconi L., Genzel R., 2004, ApJ, 602, 148
Davies R., Tacconi L., Genzel R., 2004, ApJ, 613, 781
Davies R., et al., 2006, ApJ, 646, 754
Davies R., Mueller Sánchez F., Genzel R., Tacconi L,. Hicks E., Friedrich S., Sternberg A., 2007, ApJ, 671, 1388
Davies R., et al., 2008, The ESO Messenger, 131
Dunlop J., McLure R., Kukula M., Baum S., C O'Dea S., Hughes D., 2003, MNRAS, 340, 1095
Eckart A., et al., 2006, A&A, 450, 535
Egner S., 2006, PhD Thesis, Max Planck Institute for Astronomy and the University of Heidelberg, http://www.ub.uni-heidelberg.de/archiv/6974
Eisenhauer F., et al., 2003, in *Instrument Design and Performance for Optical/Infrared Ground-based Telescopes*, eds. Masanori I., Moorwood A., Proc. SPIE, 4841, 1548
Eisenhauer F., et al., 2005, ApJ, 628, 246
Eisenhauer F., et al., 2008, in *The Power of Optical/IR Interferometry*, ed. Richichi A., Delplancke F., Paresce F., Chelli A., ESO Astrophysics Symposia, p.431
Falomo R., Kotilainen J., Scarpa R., Treves A., 2005, A&A, 434, 469
Fan X., et al., 2003, AJ, 125, 1649
Ferrarese L., Merritt D., 2000, ApJ, 539, L9
Ferrarese L., Ford H., 2005, SSRv, 116, 523
Ferrarese L., et al., 2006, ApJ, 644, L21
Fried D., 1965, JOSA, 55, 1427
Förster Schreiber N., Genzel R., Lutz D., Sternberg A., 2003, ApJ, 599, 193
Gebhardt K., et al., 2000, ApJ, 539, L13
Genzel R., et al., 2003a, ApJ, 594, 812
Genzel R., Schödel R., Ott T., Eckart A., Alexander T., Lacombe F., Rouan D., Aschenbach B., 2003b, Nature, 425, 934

Ghez A., Salim S., Hornstein S., Tanner A., Lu J., Morris M., Becklin E., Duchêne G., 2003, ApJ, 620, 744
Gillessen S., et al., 2006, ApJ, 640, L163
Gratadour D., Clénet Y., Rouan D., Lai O., Forveille T., 2003, A&A, 411, 335
Gratadour D., Rouan D., Boccaletti A., Riaud P., Clénet Y., 2005, A&A, 429, 433
Gratadour D., Rouan D., Mugnier L., Fusco T., Clénet Y., Gendron E., Lacombe F., 2006, A&A, 446, 813
Guyon O., Sanders D., Stockton A., 2006, ApJS, 166, 89
Hardy J., 1998, *Adaptive Optics for Astronomical Telescopes* (OUP)
Hartmann J., 1900, Zeitschrift für Instrumentenkunde, 20, 47
Hicks E., Malkan M., 2008 ApJS, 174, 31
Hicks E., Davies R., Mueller Sánchez F., Genzel R., Tacconi L., Friedrich S., Sternberg A., 2008, to be submitted to ApJ
Ho L., 1999, ApJ, 516, 672
Hutchings J., 2006, NewAR, 50, 685
Jaffe W., et al., 2004, Nature, 429, 47
Kasper M., 2000, PhD Thesis, Max Planck Institute for Astronomy and the University of Heidelberg
Kaspi S., Maoz D., Netzer H., Peterson B., Vestergaard M., Jannuzi B., 2005, ApJ, 629, 61
Kauffmann G., et al., 2003, MNRAS, 346, 1055
Kennicutt Jr R., 1998, ApJ, 498, 541
Kormendy J., Richstone D., 1995, ARA&A, 33, 581,
Koyama K., Maeda Y., Sonobe T., Takeshima T., Tanaka Y., Tamauchi S., 1996, PASJ, 48, 249
Kuhlbrodt B., Örndahl E., Wisotzki L., Jahnke K., 2005, A&A, 439, 497
Lacy M., 2006, in *Astrophysics Update 2*, ed. Mason J, Springer (Heidelberg, Germany)
Lai O., Rouan D., Rigaut F., Arsenault R., Gendron E., 1998, A&A, 334, 783
Magorrian J., et al., 1998, AJ, 115, 2285
Marchetti E., et al., 2007, the ESO Messenger, 129, 8
Marco O., Alloin D., 2000, A&A, 353, 465
Márquez I., Petitjean P., Théodore B., Bremer M., Monnet G., Beuzit J.-L., 2001, A&A, 371, 97
Max C., Canalizo G., Macintosh B., Raschke L., Whysong D., Antonucci R., Schneider G., 2005, ApJ, 621, 738
McLeod K., Rieke G., 1995, ApJ, 454, L77
Meisenheimer K., et al., 2007, A&A, 471, 453
Mezger P., Duschl W., Zylka R., 1996, A&ARv, 7, 289
Mueller Sanchez F., Davies R., Eisenhauer F., Tacconi L., Genzel R., Sternberg A., 2006, A&A, 454, 481
Müller Sanchez F., Davies R., Genzel R., Tacconi L., Eisenhauer F., Hicks E., Friedrich S., Sternberg A., 2008, ApJ, submitted
Neumayer N., Cappellari M., Reunanen J., Rix H.-W., van der Werf P., de

Zeeuw T., Davies R., 2007, ApJ, 671, 1329
Nolan L., Dunlop J., Kukula M., Hughes D., Boroson T., Jimenez R., 2001, MNRAS, 323, 308
Noyola E., Gebhardt K., Bergmann M., 2008, ApJ, accepted
Ozernoy L., Genzel R., 1996, in *The Unsolved Problems of the Milky Way*, ed. L. Blitz L., Teuben P. (Dordrecht: Kluwer), IAU Symp. 169, 181
Ozernoy L., Genzel R., Usov V., 1997, MNRAS, 288, 1997
Paumard T., Maillard J.-P., Morris M., Rigaut F., 2001, A&A, 366, 466
Paumard T., et al., 2006, ApJ, 643, 1011
Paumard T., et al., 2008, in *The Power of Optical/IR Interferometry*, ed. Richichi A., Delplancke F., Paresce F., Chelli A., ESO Astrophysics Symposia, p.313
Peterson B., 2001, in *Advanced Lectures on the Starburst-AGN Connection*, eds. Aretxaga I., Kunth D., Mújica R., (Singapore: World Scientific), pp. 3-67
Pollack L., Max C., Schneider G., 2007, ApJ, 660, 288
Poynier L., Macintosh B., Véran J.-P., 2007, JOSA A, 24, 2645
Prieto A., et al., 2004, ApJ, 614, 135
Prieto A., Maciejewski W., Reunanen J., 2005, AJ, 130, 1472
Ragazzoni R., Farinato J., Marchetti E., 2000, in *Adaptive Optical Systems Technology*, ed. Wizinowich P., SPIE, 4007, 1076
Revnivtsev M., et al., 2004, A&A, 425, L49
Roddier F., 1981, in *Progress in Optics*, 19, 281, ed. Wolf E. (Elsevier)
Roddier F., 1988, Applied in Optics, 27, 1223
Rouan D., Rigaut F., Alloin D., Doyon R., Lai O., Crampton D., Gendron E., Arsenault R., 1998, A&A, 339, 687
Rouan D., et al., 2004, A&A, 417L, 1
Sander D., Soifer T., Elias J., Madore B., Matthews K., Neugebauer G., Scoville N., 1988, ApJ, 325, 74
Schartmann M., PhD Thesis, Max Planck Institute for Astronomy and the University of Heidelberg
Schawinski K., Thomas D., Sarzi M., Maraston C., Kaviraj S., Joo S.-J., Yi S., Silk J., 2007, MNRAS, 382, 1415
Schwarzschild M., 1979, ApJ, 232, 236
Shack R., Platt B., 1971, JOSA, 61, 656
Sikora M., Stawarz Ł., Lasota J.-P., 2007, ApJ, 658, 815
Tedds J., Brand P., Burton M., 1999, MNRAS, 307, 337
Thomas J., et al., 2004 MNRAS, 353, 391
Thompson T., Quataert E., Murray N., 2005, ApJ, 630, 167
Tremaine S., et al., 2002, ApJ, 574, 740
Trippe S., et al., 2006, JPhCS, 54, 288
Tristram K., et al. 2007, A&A, 474, 837
Vestergaard M., 2004, ApJ, 601, 676
Walter F., Carilli C., Bertoldi F., Menten K., Cox P., Lo K., Fan X., Strauss M., 2004, ApJ, 615, L17